Design and Measurement of a Frequency Converter with SPWM Modulation of Output Voltage for a Two-Phase Induction Motor

Jan Kanuch, Peter Girovsky, Jaroslava Zilkova, Marek Pastor*
Department of Electrical Engineering and Mechatronics, Technical University of Kosice, Letna 9, 04200 Kosice, Slovakia
*jan.kanuch@tuke.sk; peter.girovsky@tuke.sk; jaroslava.zilkova@tuke.sk; *marek.pastor@tuke.sk*

***Abstract*—This paper deals with the design, implementation, and measurements of a frequency converter with bipolar sinusoidal pulse width modulation (SPWM) of output voltage for two-phase induction motors. The paper is dedicated to an analysis of the operation of a two-phase frequency converter and its implementation. The inverter has a single-phase H-bridge topology with split DC link and bipolar switching to minimise the number of components. Insulated gate bipolar transistors (IGBTs) are used in the realisation of the inverter power section. The inverter is controlled using a digital signal processor (DSP) TMS320F28335. Measurements with a 0.12 kW two-phase induction motor were performed to verify the correct operation of the inverter. The influence of the switching frequency on the motor current ripple is measured for frequencies of the first harmonic up to 100 Hz.**

***Index Terms*—Digital signal processor; IGBT transistor; Two-phase frequency converter; SPWM modulation.**

I. INTRODUCTION

At present, the three-phase induction motor is the most widely used type of motor in industrial electric drives [1]. However, low-power home appliances, such as washing machines, dishwashers, pumps, etc., most often use single-phase induction motors, as well as universal motors, which are powered as standard by single-phase alternating voltage with constant frequency. In the standard operation of single-phase motors, there are several issues of concern, such as low efficiency, low power factor, torque pulsation, etc. [2], [3].

A single-phase induction motor requires an auxiliary (i.e., second, so-called "starting") winding to generate the initial engagement torque. A capacitor is connected in series in this starting winding as standard. Therefore, the motor operates as an asymmetric two-phase induction motor powered by single-phase voltage. However, it is generally known that a single-phase induction motor with an auxiliary phase is not suitable for speed control due to the unsuitable speed characteristic. In single-phase drives with speed control, therefore, single-phase universal motors are traditionally used, where speed change is achieved by regulating the supply voltage using a triac or thyristor. However, with this type of power supply, the voltage on the motor armature and therefore also the corresponding current have a higher harmonic content [4]–[6]. The universal motor also includes a commutator on the armature, against which the carbon brushes press, so it is currently a very undesirable source of electromagnetic interference [7], [8]. Therefore, it is advantageous to gradually replace universal motors with two-phase squirrel-cage induction motors [9]–[12]. Their advantage lies in their simple construction, which will certainly be reflected mainly in the motor manufacturing costs. Two-phase induction motors do not contain a commutator, so they have a much longer service life and therefore involve lower maintenance costs compared to universal motors. However, their disadvantage is the need for a two-phase harmonic voltage supply with a phase shift of 90 degrees. Residential buildings, however, only provide a single-phase network, so the main goal of this paper is to design and implement a frequency converter that will create a two-phase harmonic voltage with the appropriate phase shift from a single-phase network [13]–[15].

In general, it is not simple to achieve high performance in drives over a wide range of operating conditions without the use of frequency converters. Therefore, much effort has been focussed on improving drive performance not only by the applied control method, but also by the pulse width modulation (PWM) strategy [16]–[20]. Digital techniques for generating PWM patterns seem to be more interesting due to the advent of microprocessor technology resulting in precision, ease of implementation, and flexibility [21], [22]. Vector pulse width modulation has long been established for a three-phase system with digital implementation [23], [24]. The traditional sinusoidal pulse width modulation (SPWM) technique has been overcome by the space-vector PWM (SVPWM) technique, which is more suitable for digital implementation [25]. The SVPWM technique is applicable to two-phase induction motor drives [26], [27]. Two-phase inverters using the SVPWM technique can generate only four space voltage vectors, but cannot generate zero vectors. A reference voltage vector located in the square locus is realised by adjusting the four space vectors.

A two-phase drive can be built using various configurations of inverters and windings. The single-phase

Manuscript received 6 January, 2023; accepted 17 April, 2023.
This work was supported by the Slovak Research and Development Agency under the Contracts Nos. APVV-16-0270, APVV-18-0436, and APVV-19-0210.

H-bridge contains around 30 % fewer components than its three-phase alternative. The variable frequency drive (VFD) with a two-phase motor can be easily created from a single-phase motor if we replace the starting capacitor with an inverter. An H-bridge inverter is one of the cheapest ways, as it uses only four switches and two capacitors connected in series to a DC power supply. The capacitor node forms the centre of the asymmetrical DC source and is connected to the node (middle point) of a two-phase winding. In practise, two resistors connected in parallel with capacitors are also used to equalise the voltage of the capacitors. However, this design increases losses in the system. The second disadvantage is that at low motor speeds, this type of converter has slightly asymmetrical operation due to uneven discharge of the DC intermediate circuit capacitors [28], [29].

The paper describes the development of a frequency converter for a two-phase motor supplied from a single-phase grid. The designed frequency converter enables effective speed control of a two-phase motor with small current and torque ripple.

The paper is organised as follows. The general description of the designed frequency converter is presented in Section II. Section III describes the implementation of the power section of the inverter. Section IV presents the design of the control algorithm and its verification, including the design of gate drivers, galvanic isolations for control signals, and auxiliary power supply. The verification of the proposed VFD with a two-phase induction motor is presented in Section V. Section VI concludes the paper.

II. Frequency Converter for Two-Phase Induction Motor

To supply a two-phase induction motor, a source of two harmonic voltages mutually phase-shifted by 90 degrees is required, which creates a rotating magnetic field in the motor [30].

The frequency inverter (Fig. 1) is powered by a single-phase supply network, the voltage of which is rectified by a single-phase rectifier. The rectified voltage is applied to a capacitive divider that performs the function of a symmetrical voltage source. The inverter power section consists of two legs with IGBT transistors and antiparallel diodes, which also form the output terminals of the inverter. The induction motor winding is connected between the output terminals of the inverter and the capacitive divider node. The power transistor in each leg can be switched on only if the second transistor in the given branch is switched off. The simultaneous turn-on of both transistors in one leg would create a short circuit, and conversely, the concurrent blocking state of both transistors would mean an indeterminate state.

The output voltages of the first harmonic of the individual legs are described by (1) and (2):

$$u_{01} = \frac{U_e}{2} + k_m \frac{U_e}{2} \sin \omega t, \tag{1}$$

$$u_{02} = \frac{U_e}{2} + k_m \frac{U_e}{2} \cos \omega t, \tag{2}$$

where U_e is the DC input voltage of the inverter and k_m is the amplitude modulation index, which indicates the ratio between the output voltage required amplitude and the DC supply voltage of the inverter and influences the maintenance of a constant ratio between the voltage and the output voltage frequency.

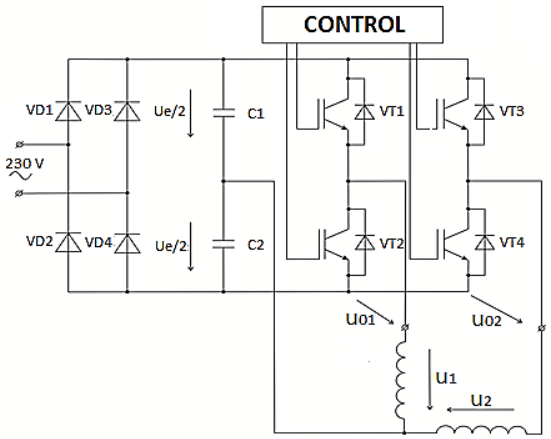

Fig. 1. Schematic diagram of the proposed two-phase converter wiring.

The first harmonic phase voltages are described by (3) and (4):

$$u_1 = u_{01} - \frac{U_e}{2} = k_m \frac{U_e}{2} \sin \omega t, \tag{3}$$

$$u_2 = u_{02} - \frac{U_e}{2} = k_m \frac{U_e}{2} \cos \omega t. \tag{4}$$

The inverter is controlled by sinusoidal pulse width modulation (SPWM) with carrier frequency (switching frequency of transistors) in the range of 1 kHz to 8 kHz. The basis of SPWM modulation is the comparison of a sawtooth carrier signal with the modulation signal, in our case with the sine and cosine signal waveforms. When the sawtooth and modulation signals coincide, pulses are generated which induce switching of the IGBT transistors in the legs of the inverter. Since in one leg there cannot be a state when both transistors are simultaneously switched on, it is necessary to create control pulses for the transistors of one leg that are negated by each other. This always results in a state in which only one transistor in a leg is turned on [31].

III. Design and Implementation of Converter Power Section

The proposed frequency converter will be used mainly for two-phase motors for low-power drives up to 500 W. For experimental purposes and to meet the measurements with the motor in limit states, the power section of the inverter has been designed for a maximum AC current I_{max} = 10 A. For the reasons mentioned above, for AC supply voltage (mains) of 230 V/50 Hz, a rectifier diode DSEI 12-06A with basic parameters of I_{FAV} = 14 A and U_{RRM} = 600 V has been used [32].

For the maximum voltage on the IGBT transistor, which is U_{CE} = 325 V, and the maximum current flowing through the transistor I_{CE} = 10 A, we used a transistor from IRF company, type IRG4BC30UD, which also integrates an

antiparallel diode, the basic parameters of which are U_{CES} = 600 V, I_C = 12 A (100 ˚C), U_{CEon} = 1,95 V [33].

Calculating the conduction losses and switching losses of a transistor depends on the duty cycle of switching. In SPWM, the duty cycle varies during the period; therefore, the analytical calculation of the total losses of the transistor is complicated [34], [35]. Therefore, the Orcad PSpice simulation programme, which includes a model of the IRG4BC30UD transistor, was used to determine the magnitude of the total losses that were used for the heatsink design.

The design of the capacitive voltage divider was based on the maximum voltage on the capacitive voltage divider U_e = 326 V, and thus the voltage on one capacitor is $U_e/2$ = 163 V. The capacitance of the capacitors was determined by simulation to be C = 2000 µF. The capacitor used in the implementation was a type TME capacitor ALS31A222MF400, 2200 µF/450 V with dimensions ø66 × 105 mm.

The realised module of the two-phase frequency converter is shown in Fig. 2.

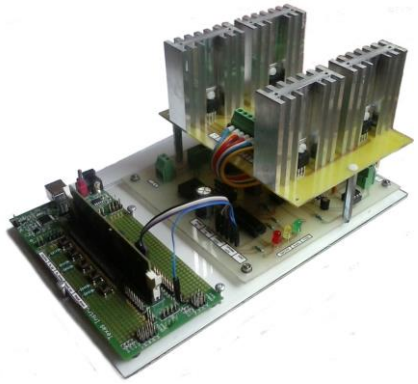

Fig. 2. Design solution of a frequency converter for two-phase induction motors.

IV. Design and Implementation of Inverter Power Section Control

The inverter power section control is performed by a digital signal processor TMS320F28335 (hereinafter referred to as DSP) from Texas Instruments. Signal processors currently achieve relatively high computational power and include peripherals that enable the control of complex systems.

The basic DSP TMS320F28335 peripherals include [36], [37]:

– 3 off 32-bit central processor unit (CPU) timer;
– 6 off PWM modules;
– 6 off capture modules;
– 2 off QEP modules;
– 1 off 12-bit A/D inverter;
– General purpose input/output (GPIO) interface [32].

Each PWM peripheral includes two independent PWM outputs (ePWMA and ePWMB).

A. Basic Inverter Control Algorithm

After starting the inverter control programme, the frequency of the output voltage modulation signal (f_u = 50 Hz) and the frequency of the carrier signal (f_c = 2 kHz) are set. The frequency of the inverter output voltage can be varied in the range of 5 Hz–100 Hz in 5 Hz steps, and the frequency of the carrier signal in the range of 1 kHz–8 kHz in 0.5 kHz steps.

Because the voltage at the inverter output cannot drop to 0 V, the modulation coefficient must be limited to k_m = 0.1, which means that up to the minimum frequency f_u = 10 Hz, there will be a constant voltage at the inverter output, the magnitude of which will be 10 % of the inverter supply voltage.

The control signals from the DSP at frequency f_u = 100 Hz and the carrier signal frequencies (identical to the switching frequency f_{sw}) f_c = 2 kHz are shown in Fig. 3.

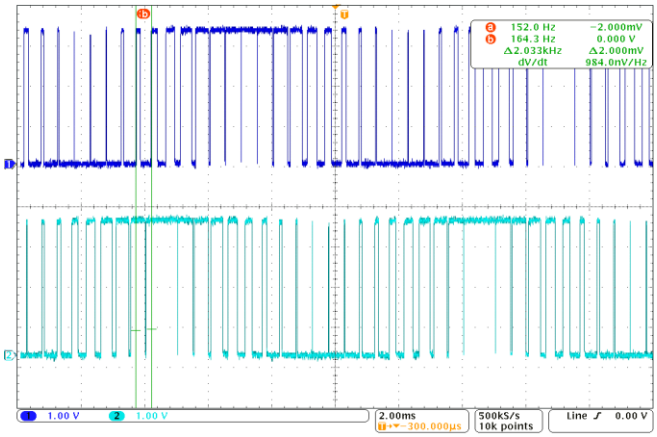

Fig. 3. DSP output control signal with frequency f_u = 100 Hz and carrier frequency f_c = 2 kHz.

B. Power Transistor Driver

To turn on the IGBT transistors, an appropriate switching pulse is required, which is provided by the IR2111 drivers by International Rectifier. The advantage of these drivers is that for complementary switching of the transistors, it is sufficient to supply switching pulses for only one of the transistor pairs. The driver logic automatically creates switching signals at the driver output with dead time for both transistors, simplifying the resulting control circuit. The power supply for the drivers is 15 V and the logic level is 9 V. To provide galvanic isolation of the power section from the control section of the inverter, it is necessary to separate the control ground from the driver ground. For the excitation of the upper transistors, it is not necessary to generate a separate supply voltage because the drivers use the so-called "bootstrap circuit" to generate the voltage required for the control electrodes of the IGBT transistors. The driver wiring diagram is shown in Fig. 4 [38], [39].

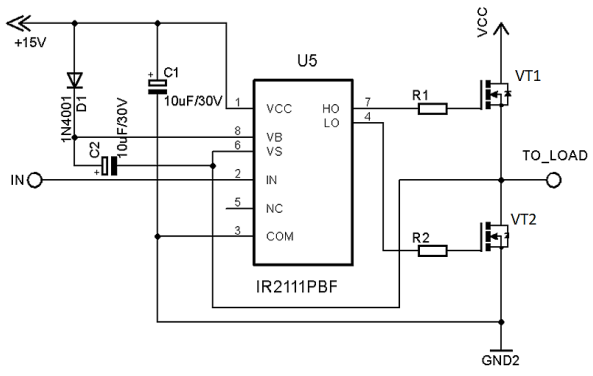

Fig. 4. IR2111PBF driver wiring diagram.

C. Galvanic Isolation of the Control from the Power Section of the Inverter

Galvanic isolation is achieved with the LTV827 optocoupler, which contains a pair of diodes and phototransistors. To maintain galvanic isolation, it is necessary to separate the ground level of the DSP at the optocoupler input from the ground level of the drivers at the optocoupler output. To fully open the phototransistor at the optocoupler output, the diode needs to be supplied with a voltage of 5 V, so the voltage level from the DSP needs to be amplified through the 74LS541N bus driver. For proper operation of the optocoupler, it is necessary to calculate the resistor values so that the diode and phototransistor current reach the value Id = IT = 40 mA. The circuit also contains a light emitting diode (LED) diode to indicate the status of the incoming pulses from the DSP. The circuit diagram is shown in Fig. 5.

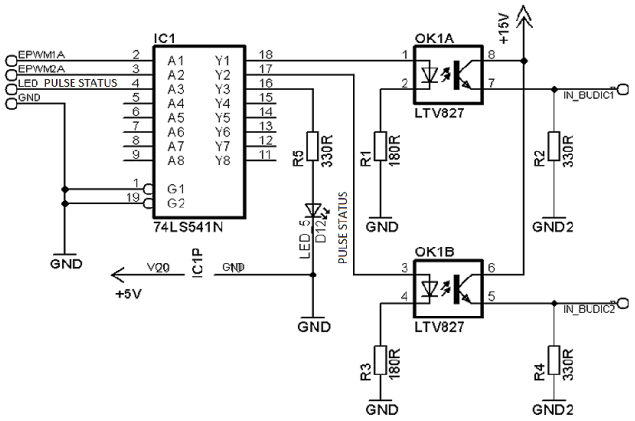

Fig. 5. Galvanic isolation of the control from the power section of the inverter.

D. Inverter Control

The control switches TL1 to TL4 are located directly on the DSP docking board. Switches TL1 (fu_up) and TL2 (fu_down) are used to change the frequency of the inverter output voltage in 5 Hz steps. Switches TL3 (fmod_up) and TL4 (fmod_down) change the inverter switching frequency in 0.5 kHz steps. The switches are connected between the individual inputs and the GND of the signal processor via the resistors R = 330 Ω. For proper operation of the control, the internal PULL_UP resistors in the GPIO registers must be enabled. The ePWM1A and ePWM2A output control pulses are set as PWM outputs in the GPIO registers.

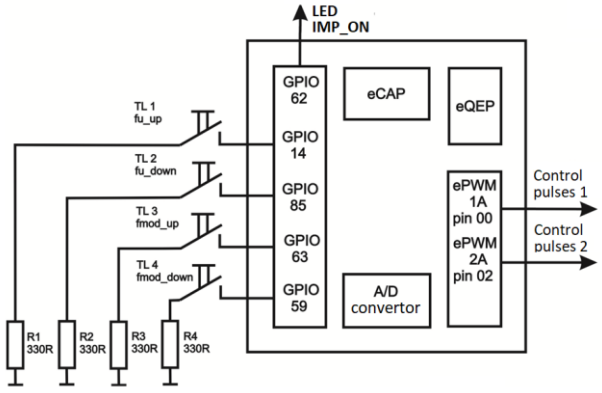

Fig. 6. Control wiring diagram.

The block diagram of the control wiring is shown in Fig. 6 [40].

E. Overall Wiring Diagram and Realisation of the Control Section of the Inverter

The overall wiring diagram is shown in Fig. 7. This diagram consists of the circuits that have been described in the previous subchapters. In the implementation, a single-sided printed circuit board (PCB) with dimensions 120 mm × 130 mm was used. The PWM control pulses along with the DSP zero potential are applied to the 74LS541N bus driver through a set of input connectors. The connection of the output switching signals from the IR2111 drivers to the inverter power board is made using an output terminal block. The COM terminal (driver ground) is common for both drivers. The power supply transformer is located directly on the control PCB.

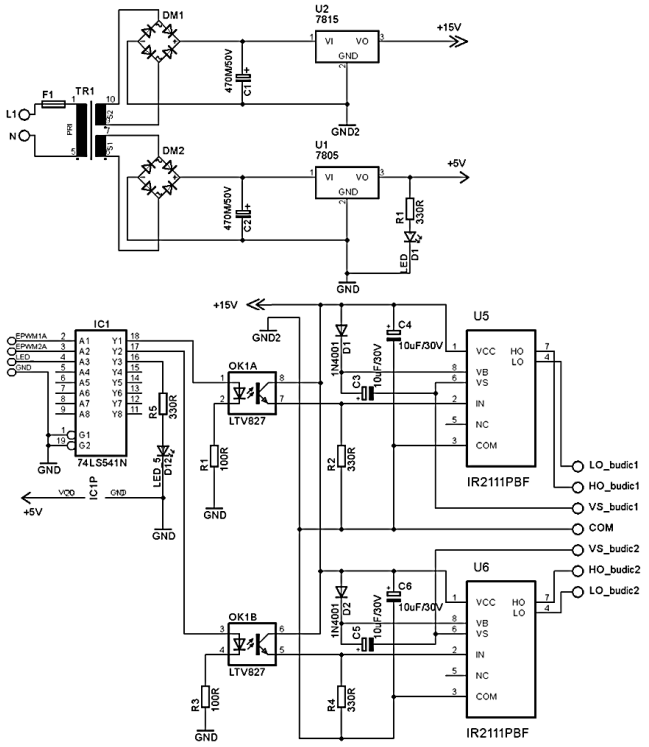

Fig. 7. Overall inverter control wiring diagram.

V. VERIFICATION OF THE FUNCTIONALITY AND CHARACTERISTICS OF THE INVERTER BY MEASUREMENT

A laboratory power source with a voltage of 2×100 V/3 A was used to supply the frequency converter inverter. A two-phase squirrel-cage induction motor designed and manufactured for this purpose [41] was connected to the inverter output. The motor has two identical two-pole concentric windings that are offset from each other by 90 degrees. The motor parameters are given in Table I.

TABLE I. TWO-PHASE INDUCTION MOTOR PARAMETERS.

Parameter	Value
Voltage	2×230 V
Power	0.12 kW
Current	0.7 A
Frequency	50 Hz
Motor speed	2580 rpm
Power factor	0.74
Motor torque	0.44 Nm

A ZES ZIMMER LMG500 precision power analyser was used to measure the voltage values in the individual phases of the induction motor. Because only the voltmeter function was used, the power analyser is depicted as two digital voltmeters PV_1 and PV_2 in Fig. 8. The waveforms of the induction motor voltages and currents were recorded by a Tektronix MSO4034 digital oscilloscope. The motor speed was measured by a contactless laser speed sensor. The wiring diagram of the power part of the measurement is shown in Fig. 8. The power was not measured as it is a more complex task due to the non-sinusoidal two-phase system, which has the zero-sequence component [42], [43].

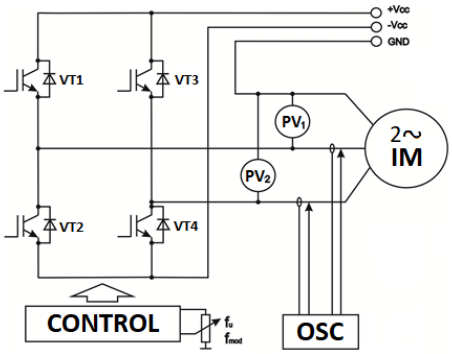

Fig. 8. Measurement circuit schematic.

The voltage and current waveforms in the individual motor phases were measured at various inverter output voltage frequencies and various frequency modulation indexes to show the effect of the frequency modulation index on the output ripple current. Another goal of the measurement was to verify the correct operation of the inverter control while maintaining a constant output voltage-to-frequency ratio. The performance of the control technique with regard to the current ripple of the motor's currents was verified as well.

Figure 9 illustrates how the pulse width changes during each period due to SPWM modulation. After filtering the voltage with an RC filter with parameters R =1 kΩ and C = 330 nF, both inverter output voltages in Fig. 10 have a sinusoidal waveform with a phase shift of 90 °. Using a digital voltmeter, phase voltages $U_{L1} = U_{L2} = 38.3$ V (rms) were measured. The switching frequency of the inverter f_{sw} = 2 kHz is quite small, resulting in a significantly rippled motor current, as illustrated in Fig. 11.

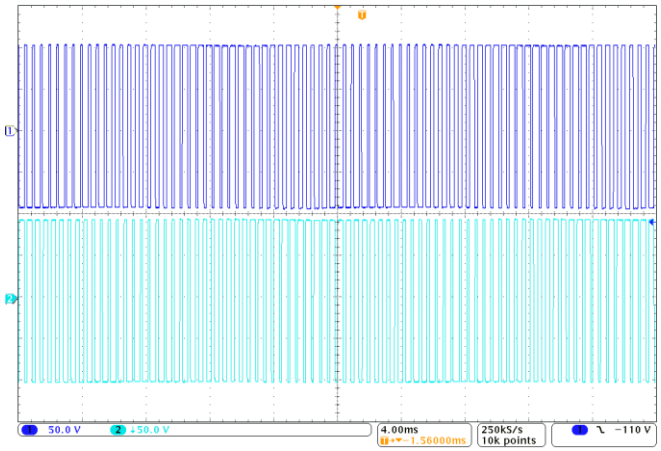

Fig. 9. Voltage waveforms on motor phases at f_u = 50 Hz and f_{sw} = 2 kHz.

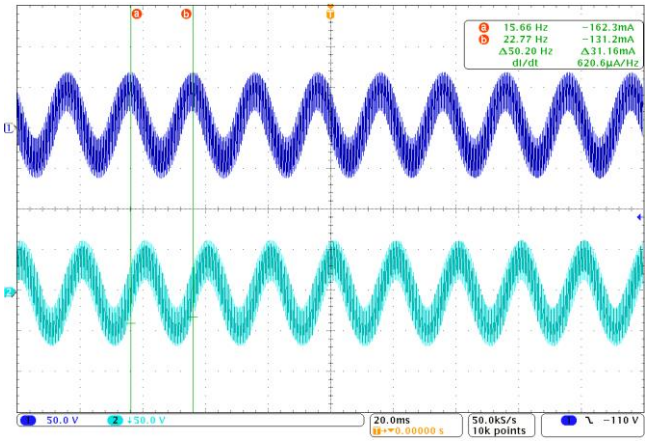

Fig. 10. Voltage waveforms on motor phases at f_u = 50 Hz and f_c = 2 kHz using an RC filter.

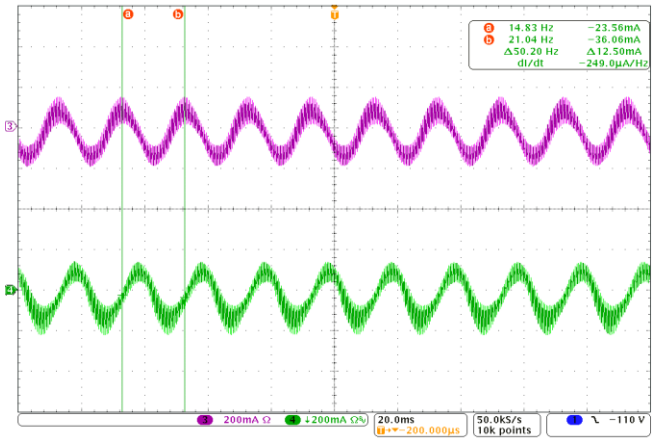

Fig. 11. Current waveforms on motor phases at f_u = 50 Hz and f_c = 2 kHz.

At frequency f_u = 100 Hz, the modulation index of amplitude is equal to one, which means that the amplitude of the first harmonic of the output voltage reaches the maximum value. This phenomenon can be seen in Fig. 12, where there are sections in which the transistors do not manage to be switched off or on in time. This occurs when the amplitude of the comparator signal is the same as the amplitude of the sawtooth signal. The voltage amplitude in Fig. 13 reaches 100 V, which is twice the value of the voltage in Fig. 10, where the amplitude is equal to 50 V. Phase voltages $U_{L1} = U_{L2} = 72.5$ V (rms) were measured with a digital voltmeter. From the above, it can be concluded that the control maintains a constant ratio of output voltage and output frequency of the inverter. A constant current with an amplitude of 180 mA was flowing through the motor at both supply voltage frequencies.

At the frequency of f_u = 50 Hz, after increasing the carrier frequency to f_c = 8 kHz, a significant reduction in the motor current ripple can be seen in Fig. 14. The reduction in current ripple is due to the fourfold increase in the number of transistor switchings during one period. Phase voltages $U_{L1} = U_{L2} = 40.5$ V (rms) were measured with a digital voltmeter. The waveforms of motor voltages and currents at frequencies f_u = 100 Hz and f_c = 8 kHz are shown in Figs. 15–17.

At the frequency f_u = 100 Hz and after increasing the carrier frequency to f_c = 8 kHz, the phase voltages $U_{L1} = U_{L2}$ = 74.3 V (rms) were measured with a digital voltmeter. It

can be concluded that even when the modulation frequency was changed, the motor maintained a constant output voltage-to-frequency ratio.

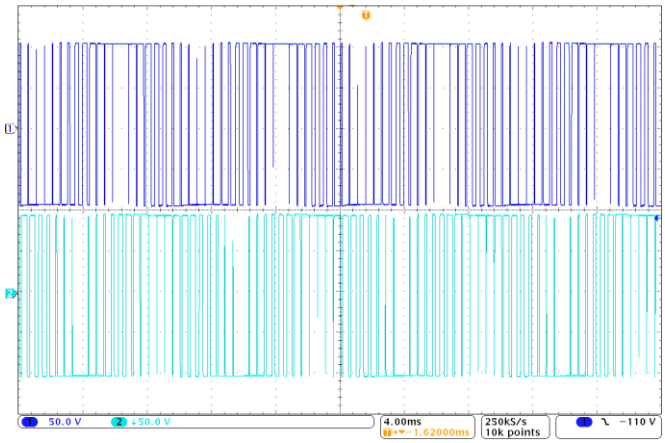

Fig. 12. Voltage waveforms on motor phases at f_u = 100 Hz and f_c = 2 kHz.

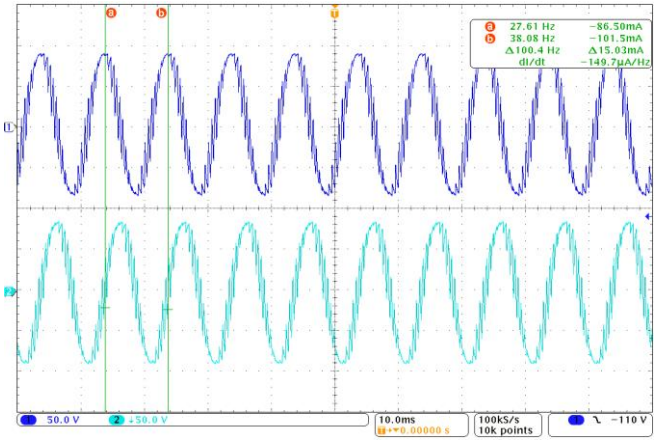

Fig. 13. Voltage waveforms on motor phases at f_u = 100 Hz and f_c = 2 kHz using an RC filter.

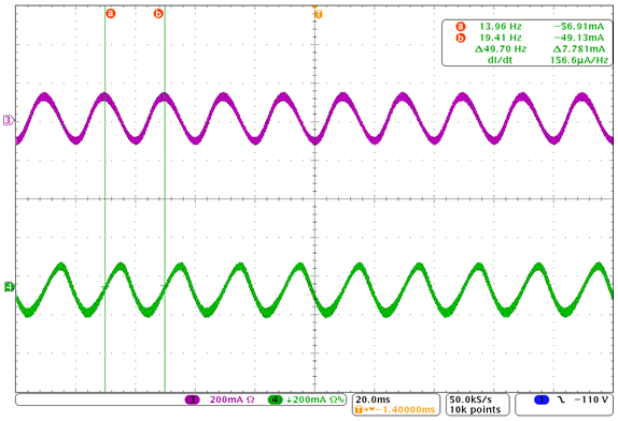

Fig. 14. Current waveforms on motor phases at f_u = 50 Hz and f_c = 8 kHz.

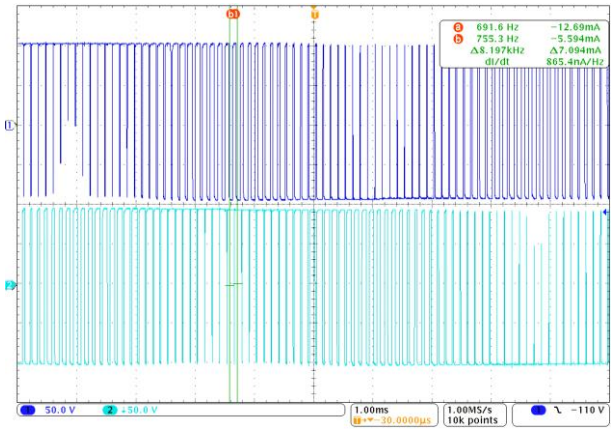

Fig. 15. Voltage waveforms on motor phases at f_u = 100 Hz and f_c = 8 kHz.

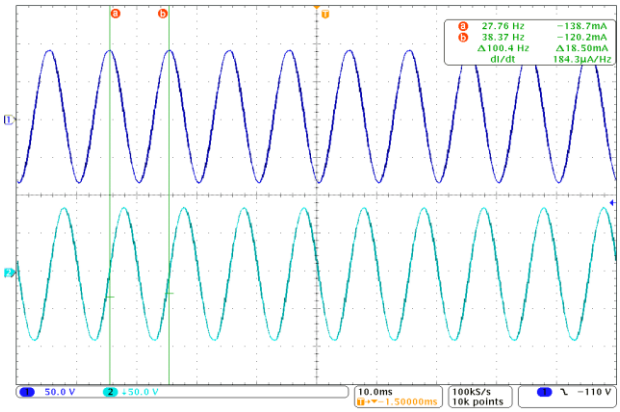

Fig. 16. Voltage waveforms on motor phases at f_u = 100 Hz and f_c = 8 kHz using an RC filter.

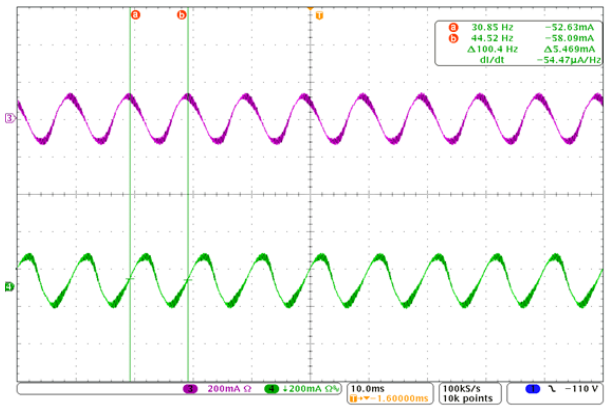

Fig. 17. Current waveforms on motor phases at f_u = 100 Hz and f_c = 8 kHz.

VI. CONCLUSIONS

This paper describes the design and implementation of a frequency converter for powering two-phase motors up to 500 W. The functionality of the converter has been verified by measurements. The power section of the inverter consists of two legs with two IGBT transistors and antiparallel diodes. Inverter control is performed using a digital signal processor (DSP). The DSP generates control pulses for the IGBT transistors based on SPWM modulation. The inverter control enables a change in the frequency of the inverter output voltage and the modulation frequency. Auxiliary control circuits are used to connect the DSP and the power part of the inverter.

The designed frequency converter was tested with a loaded two-phase induction motor of 0.12 kW specially designed and manufactured for this purpose. From the measured voltage and current waveforms from the oscilloscope of the inverter, it can be concluded that the designed converter meets the set requirements. The converter makes it possible to change the frequency of the output voltage, i.e., the supply voltage of the motor, while maintaining a constant ratio of output voltage and frequency at different switching frequencies, thus avoiding the

increase of magnetising current in the motor. Changing the switching frequency affects the ripple current. At higher switching frequencies, when the number of transistor switchings per period increases, the motor current has a smoother waveform.

The control of the inverter is bipolar; in the future, it is possible to add another leg of IGBT transistors to the power section of the inverter and to modify the control to unipolar, thus achieving a smaller number of higher harmonics in the output voltage of the inverter. The experimental measurement results demonstrate that the converter described in this paper meets the desired requirements and can be implemented in practise.

CONFLICTS OF INTEREST

The authors declare that they have no conflicts of interest.

REFERENCES

[1] G. B. Lucas, B. A. de Castro, M. A. Rocha, and A. L. Andreoli, "Three-phase induction motor loading estimation based on Wavelet Transform and low-cost piezoelectric sensors", *Measurement*, vol. 164, pp. 1–10, 2020. DOI: 10.1016/j.measurement.2020.107956.

[2] C.-M. Young, C.-C. Liu, and C.-H. Liu, "New inverter-driven design and control method for two-phase induction motor drives", *IEE Proc. - Electric Power Applications*, vol. 143, no. 6, pp. 458–466, 1996. DOI: 10.1049/ip-epa:19960526.

[3] F. Blaabjerg, F. Lungeanu, K. Skaug, and M. Tonnes, "Evaluation of low-cost topologies for two phase induction motor drives", *Conf. Rec. of the IEEE Industry Applications Conference. 37th IAS Annual Meeting*, 2002, pp. 2358–2365. DOI: 10.1109/IAS.2002.1042775.

[4] D. G. Holmes and A. Kotsopoulos, "Variable speed control of single and two phase induction motors using a three phase voltage source inverter", *Conf. Rec. of the IEEE Industry Applications Conference Twenty-Eighth IAS Annual Meeting*, 1993, pp. 613–620. DOI: 10.1109/IAS.1993.298887.

[5] M. F. Rahman and L. Zhong, "A current-forced reversible rectifier fed single-phase variable speed induction motor drive", *PESC Record. 27th Annual IEEE Power Electronics Specialists Conference*, 1996, pp. 114–119, vol. 1. DOI: 10.1109/PESC.1996.548568.

[6] M. B. R. Correa, C. B. Jacobina, A. M. N. Lima, and E. R. C. Da Silva, "Field oriented control of a single-phase induction motor drive", *PESC 98 Record. 29th Annual IEEE Power Electronics Specialists Conference*, 1998, pp. 990–996. DOI: 10.1109/PESC.1998.703124.

[7] J. Kanuch and P. Visnyi, "EMC of universal DC motor", *Zeszyty Problemove - Maszyny Elektryczne*, no. 88, pp. 209–215, 2010.

[8] N. Yuta, A. Yuji, and U. Dai, "EMC measure examination of an ultra high-speed powerd universal motor", *Papers of Technical Meeting on Rotating Machinery*, vol. RM-06, no. 124–144, pp. 7–10, 2006.

[9] S. Valtchev, O. V. Kryukov, V. N. Meshcheryakov, and A. S. Belousov, "Comparative analysis of electric drives control systems applied to two-phase induction motors", in *Proc. of 2020 2nd International Conference on Control Systems, Mathematical Modeling, Automation and Energy Efficiency (SUMMA)*, 2020, pp. 918–922. DOI: 10.1109/SUMMA50634.2020.9280637.

[10] V. Meshcheryakov and A. Belousov, "Development of a method for reducing starting currents and electromagnetic torque of a two-phase induction motor by delaying voltage supply", in *Proc. of 2021 XVIII International Scientific-Technical Conference Alternating Current Electric Drives (ACED)*, 2021, pp. 1–5. DOI: 10.1109/ACED50605.2021.9462269.

[11] A. S. Belousov, V. N. Meshcheryakov, S. Valtchev, and O. V. Kryukov, "Start and reverse of single-phase and two-phase induction motors", in *Proc. of 2021 3rd International Conference on Control Systems, Mathematical Modeling, Automation and Energy Efficiency (SUMMA)*, 2021, pp. 1135–1140. DOI: 10.1109/SUMMA53307.2021.9632128.

[12] V. K. Pandey, M. Kumar, M. B. Patil, A. K. Pandey, R. D. Kulkarni, and V. K. Shaima, "Design, modeling and simulation of two-phase induction motor integrated with inverter drive", in *Proc. of 2021 2nd Global Conference for Advancement in Technology (GCAT)*, 2021, pp. 1–8. DOI: 10.1109/GCAT52182.2021.9587854.

[13] J. Kanuch and P. Visnyi, "Control of two-phase induction motor using a conventional three-phase bridge inverter", *Zeszyty Problemove - Maszyny Elektryczne*, no. 100, pp. 171–174, 2013.

[14] Ch. Charumit and V. Kinnares, "Carrier-based unbalanced phase voltage space vector PWM strategy for asymmetrical parameter type two-phase induction motor drives", *Electric Power Systems Research*, vol. 79, no. 7, pp. 1127–1135, 2009. DOI: 10.1016/j.epsr.2009.02.003.

[15] J. Přibil, M. Kamenský, and J. Vlnka, "Návrh ovládania asynchrónneho motora pomocou frekvenčného meniča a PC (in Slovak)", *Mechanik Elektrotechnik: 3. ročník*, pp. 28–30, 2009.

[16] S. Sinthusonthichat and V. Kinnares, "A new modulation strategy for unbalanced two phase induction motor drives using a three-leg voltage source inverter", *IEEJ Trans. Ind. Appl.*, vol. 125, no. 5, pp. 482–491, 2005. DOI: 10.1541/ieejias.125.482.

[17] E. R. Benedict and T. A. Lipo, "Improved PWM modulation for a permanent-split capacitor motor", *Conference Record of the 2000 IEEE Industry Applications Conference. Thirty-Fifth IAS Annual Meeting and World Conference on Industrial Applications of Electrical Energy (Cat. No.00CH37129)*, 2000, pp. 2004–2010. DOI: 10.1109/IAS.2000.882152.

[18] J. Yao, J. Krase, and T. A. Lipo, "Design considerations for motor-controller integration of a single phase induction motor packaged drive", in *Proc. of IEEE International Electric Machines and Drives Conference*, 2003, pp. 1239–1244, vol. 2. DOI: 10.1109/IEMDC.2003.1210398.

[19] D. Perdukova, P. Fedor, V. Fedák, and S. Padmanaban, "Lyapunov based reference model of tension control in a continuous strip processing line with multi-motor drive", *Electronics*, vol. 8, no. 1, p. 60, 2019. DOI: 10.3390/electronics8010060.

[20] M. Leso, J. Zilkova, M. Pastor, and J. Dudrik, "Fuzzy logic control of soft-switching DC-DC converter", *Elektronika ir Elektrotechnika*, vol. 22, no. 5, pp. 3–7, 2016. DOI: 10.5755/j01.eie.22.5.16334.

[21] P. K. Sadhu, G. Sarkar, and A. Rakshit, "A microcontroller-based variable voltage variable frequency sinusoidal power source with a novel PWM generation strategy", *Measurement*, vol. 45, no. 1, pp. 59–67, 2012. DOI: 10.1016/j.measurement.2011.09.024.

[22] A. Ibrahim and M. Z. Sujod, "Variable switching frequency hybrid PWM technique for switching loss reduction in a three-phase two-level voltage source inverter", *Measurement*, vol. 151, pp. 1–8, 2020. DOI: 10.1016/j.measurement. 2019.107192.

[23] M. Leso, J. Zilkova, and P. Girovsky, "Development of a simple fuzzy logic controller for DC-DC converter", in *Proc. of IEEE 18th International Power Electronics and Motion Control Conference (PEMC)*, 2018, pp. 86–93. DOI: 10.1109/EPEPEMC.2018.8521896.

[24] M. B. de R. Correa, C. B. Jacobina, A. M. N. Lima, and E. R. C. da Silva, "A three-leg voltage source inverter for two-phase AC motor drive systems", *IEEE Trans. on Power Electronics*, vol. 17, no. 4, pp. 517–523, 2002. DOI: 10.1109/TPEL.2002.800984.

[25] J. A. Bosnic, M. Despalatovic, G. Petrovic, and G. Majic, "Non-sinusoidal voltage generator controlled by space vector PWM", *Measurement*, vol. 150, pp. 13–18, 2020. DOI: 10.1016/j.measurement.2019.107088.

[26] D.-H. Jang and D.-Y. Yoon, "Space-vector PWM technique for two-phase inverter-fed two-phase induction motors", *IEEE Transactions on Industry Applications*, vol. 39, no. 2, pp. 542–549, 2003. DOI: 10.1109/TIA.2003.809448.

[27] D. Perduková, P. Palacký, P. Fedor, P. Bober, and V. Fedák, "Dynamic identification of rotor magnetic flux, torque and rotor resistance of induction motor", *IEEE Access*, vol. 8, pp. 142003–142015, 2020. DOI: 10.1109/ACCESS.2020.3013944.

[28] M. A. Jabbar, A. M. Khambadkone, and Z. Yanfeng, "Space-vector modulation in a two-phase induction motor drive for constant-power operation", *IEEE Transactions on Industrial Electronics*, vol. 51, no. 5, pp. 1081–1088, 2004. DOI: 10.1109/TIE.2004.834969.

[29] N. M. B. Abdel-Rahim and A. Shaltout, "An unsymmetrical two-phase induction motor drive with slip-frequency control", *IEEE Transactions on Energy Conversion*, vol. 24, no. 3, pp. 608–616, 2009. DOI: 10.1109/TEC.2009.2026599.

[30] F. Blaabjerg, F. Lungeanu, K. Skaug, and M. Tonnes, "Two-phase induction motor drives", *IEEE Industry Applications Magazine*, vol. 10, no. 4, pp. 24–32, 2004. DOI: 10.1109/MIA.2004.1311160.

[31] P. Záskalický and L. Schreier, "Using Fourier analysis for torque estimation of two-phase induction motor supplied by halfbridge inverter with PWM control", *Communications - Scientific Letters of the University of Žilina*, vol. 15, no. 3, pp. 73–78, 2013. DOI: 10.26552/com.C.2013.3.73-78.

[32] DSEI 12-06 Fast recovery diode. [Online]. Available: http://datasheet.octopart.com/DSEI12-06A-IXYS-datasheet-8612059.pdf
[33] IRG4BC30UD IGBT transistor. [Online]. Available: http://www.irf.com/product-info/datasheets/data/irg4bc30ud.pdf
[34] J. Dudrík, "Konštrukcia a dimenzovanie meničov (in Slovak)", lectures, 2013.
[35] H. Cicekli and A. Gokcen, "MOS-C Based Electronically Tuneable Current/Voltage-Mode Third Order Quadrature Oscillator and Biquadratic Filter Realization", *Elektronika ir Elektrotechnika*, vol. 27, no. 3, pp. 38-49, Jun. 2021. DOI: 10.5755/j02.eie.28921.
[36] Data manual TMS320F28335. [Online]. Available: http://www.ti.com/lit/ds/symlink/tms320f28335.pdf
[37] Enhanced Pulse Width Modulator (ePWM) modul TMS320F28335. [Online]. Available: https://www.ti.com/lit/ug/sprug04c/sprug04c.pdf?ts=1687303173811
[38] IR2111 Half-bridge driver. [Online]. Available: http://www.irf.com/product-info/datasheets/data/ir2111.pdf
[39] J. Kaňuch and P. Girovský, "Motor for direct drive of electric wheelchair", *International Journal of Engineering Research in Africa*, vol. 31, pp. 94–103, 2017. DOI: 10.4028/wwwscientific.net/JERA.31.94.
[40] System Control and Interrups TMS320F28335. [Online]. Available: http://www.ti.com/lit/ug/sprufb0d/sprufb0d.pdf
[41] J. Kanuch and Z. Ferkova, "Two-phase induction motor", in *Proc. of 12th International Conference on Low Voltage Electrical Machines*, 2012, pp. 104–107.
[42] L. Cristaldi, A. Ferrero, and R. Ottoboni, "Power and current components measurement in three-phase systems under nonsinusoidal conditions", *Measurement*, vol. 12, no. 3, pp. 251–273, 1994. DOI: 10.1016/0263-2241(94)90031-0.
[43] S. Karrer, "Measurement and simulation of induction motor characteristics", *Measurement*, vol. 7, no. 3, pp. 134–140, 1989. DOI: 10.1016/0263-2241(89)90041-9.